1    Parent material and climate interact to control soil C dynamics on annual to centennial

2              timescales through the development of poorly crystalline metal oxides

3      Jeffrey Beem-Miller[1], Craig Rasmussen[2], Alison M. Hoyt[1,3], Marion Schrumpf[1], Georg

4                              Guggenberger[4], & Susan Trumbore[1]

5    [1] Department of Biogeochemical Processes, Max Planck Institute for Biogeochemistry, Jena,

6                                              Germany

7      [2] Department of Environmental Science, The University of Arizona, Tucson, AZ, USA

8      [3] Department of Earth System Science Science, Stanford University, Stanford, CA, USA

9          [4] Institute of Soil Science, Leibniz University Hannover, Hannover, Germany

10                                  Abstract

11     Lorem ipsum. . .

Parent material and climate interact to control soil C dynamics on annual to centennial timescales through the development of poorly crystalline metal oxides

**Key messages:**

- Climate explains more variance in $\Delta^{14}C$ at the soil surface; parent material explains more variance at depth
- Interaction of parent material and climate explains more variance in bulk soil and respired $\Delta^{14}C$ than either factor alone
- Poorly crystalline metal oxide content is highly correlated with the difference between bulk soil and respired $\Delta^{14}C$

## Introduction

Understanding the response of soil carbon stocks to current and future changes in climate requires insight into both the physical and environmental factors governing soil carbon dynamics. Climate, and in particular temperature, has been found to be the most important variable for explaining the age of soil carbon in topsoil at local to global scales [Frank et al., 2012; Mathieu et al., 2015; Shi et al. 2020]. Yet our current understanding of soil organic matter decomposition underscores the importance of physical mechanisms that can affect the temperature sensitivity of decomposition, such as the interaction between soil organic matter and minerals [Davidson et al., 2000; Davidson and Janssens, 2006; Rasmussen et al., 2006; Lehmann and Kleber, 2015;]. The effect of mineral-organic associations on the temperature sensitivity of soil organic matter has been addressed in several modeling studies [Abramoff et al., 2019; Riley et al., 2016; Ahrens et al., 2015; Woolf and Lehmann, 2019]. These models typically invoke Michaelis Menten kinetics in addition to an Arrhenius-type temperature response in order to account for energy and substrate limitations on decomposition rates for soil organic matter found in association with minerals [Tang and Riley, 2019; Ahrens et al., 2020]. Studies comparing the relative importance of different soil mineral assemblages versus temperature for explaining soil C dynamics over time *in situ* are

38 scarce, yet critical for testing these model-based findings. We designed the current study to

39 quantify the relative importance of climatic versus mineralogical mechanisms of soil organic

40 C persistence across a combined gradient of mean annaul temperature (MAT) and parent

41 material in order to provide insight into the relevant time scales associated with these

42 mechanisms.

43      The relevance of soil minerals for mediating soil organic matter protection has been

44 found to be a function of the specific minerals present, rather than the amount of clay or

45 total mineral surface area [Rasmussen et al. 2018a, "Beyond Clay"]. Soil mineral assemblages

46 are dynamic, developing over time as primary minerals inherited from parent material

47 weather to form reactive, poorly crystalline secondary minerals, which in turn eventually

48 weather to increasing stable crystalline species [Slessarev 2022, others...]. Soils enriched in

49 poorly crystalline metal oxides, such as Al and Fe oxyhydroxides, are known to be of

50 particular importance for the accumulation and persistence of soil C [Torn 1997, Maseiello

51 2004]. The amount of these minerals present is directly related to parent material, but is also

52 a function of primary mineral weathering rates [Slesserav et al. 2022]. Due to the strong

53 effect of climate on weathering rates, different soil mineral assemblages can form from the

54 same parent material under different climatic regimes (Rasmussen et al. 2018b). Conversely,

55 similar mineral assemblages can be found among soils developed on different parent

56 materials given adequate time for weathering and similar vegetation and climate [Graham

57 and O'Geen 2010 "Soil mineralogy trends in California landscapes"]. These differential

58 outcomes demonstrate that climatic and mineralogical controls on soil C cycling are not

59 independent, but interact over the centennial to millenial time scales of soil development.

60      The strength and sorptive capacity of soil minerals is dependent on ligand exchange,

61 which is a function of not only surface area and charge, but more specifically the density of

62 accessible hydroxyl groups (Kaiser and Guggenberger, 2003; Rasmussen et al., 2018a

63 "Beyond Clay"; Kleber et al., 2015). Poorly crystalline metal oxides are particularly enriched

⁶⁴ in hydroxyl groups, and batch sorption/desorption experiments have shown that the

⁶⁵ mineral-organic interactions between pedogenic metal oxide-rich clays are stronger than

⁶⁶ those with siloxane-rich phyllosilicate clays (Kahle et al., 2004). Furthermore, the reactive

⁶⁷ properties of pedogenic metal oxides can also facilitate lower strength interactions with soil

⁶⁸ organic matter through multivalent cation bridging (Kleber et al., 2007). This high

⁶⁹ reactivity of poorly crystalline Fe oxides is also implicated in the observations that poorly

⁷⁰ crystalline Fe is correlated with aggregate stability but crystalline Fe oxide content is not

⁷¹ (Duiker et al., 2003). The importance of pedogenic metal oxides for explaining both soil C

⁷² concentration and bulk soil radiocarbon ($\Delta^{14}C_{bulk}$) is confirmed by the findings of

⁷³ Rasmussen et al. (Soil systems, 2018a) [other citations?], who observed that oxalate

⁷⁴ extractable iron was the best predictor of both properties. However, the relevance of

⁷⁵ mineral-organic associations with specific mineral phases such as poorly crystalline metal

⁷⁶ oxides or crystalline metal oxides for specific timescales of soil C turnover is poorly studied.

⁷⁷      Radiocarbon ($^{14}C$) is a useful tracer for soil C dynamics over time scales ranging from

⁷⁸ annual to millennial. The use of $^{14}C$ to measure timescales of soil carbon decomposition is

⁷⁹ reliant on our knowledge of the ratio of $^{12}C/^{14}C$ in the atmosphere. Once $CO_2$ is fixed into

⁸⁰ organic matter via photosynthesis, this ratio starts to shift as $^{14}C$ is preferentially lost due to

⁸¹ radioactive decay. Changes in the $^{12}C/^{14}C$ ratio due to radioactive decay are detectable at

⁸² the relatively longer timescales of hundreds to thousands of years. However, we can detect

⁸³ changes in $^{14}C$ with nearly annual resolution for the so-called "bomb-C" period, which began

⁸⁴ with the deployment and atmospheric testing of nuclear weapons in the mid-20th century.

⁸⁵ This pulse of "bomb-C" led to a doubling of atmospheric $^{14}C$ concentration prior to the ban

⁸⁶ on above-ground nuclear tests in 1963. The level of $^{14}C$ in the atmosphere returned to

⁸⁷ pre-bomb levels around 2020 (Hua et al., 2021), thus archived samples now represent the

⁸⁸ best opportunity to construct a high-resolution time series of the bomb-C pulse as it moves

⁸⁹ through different soil organic matter pools.

Soil is an open system, and this has important implications for the interpretation of radiocarbon measurements of soil C. For most soils, the majority of carbon that enters the soil leaves relatively quickly, with only a small fraction persisting (Sierra et al. 2018). Radiocarbon measurements of bulk soil C ($\Delta^{14}C_{bulk}$) typically capture the signal from these persistent pools, while more transient pools dominate measurements of C leaving the soil via heterotrophic respiration (Trumbore 2000). Here we define "transient" for C cycling on annual to decadal timescales, while we use "persistent" to refer to C cycling on centennial to millennial timescales. A diagnostic feature of the radiocarbon measurements of $\Delta^{14}C_{bulk}$ and heterotrophically respired $CO_2$ ($\Delta^{14}C_{respired}$) is that when these two signals are the same it indicates that all of the C in the soil has an equal probability of being decomposed by microbes and the system is homogenous. However, when $\Delta^{14}C_{bulk}$ and $\Delta^{14}C_{respired}$ are substantially different this indicates the presence of both labile and persistent pools of soil C.

We turned to the western slope of the Sierra Nevada Mountains, USA to compare and contrast the effects of climate and mineral assemblage on soil C dynamics. Drawing on earlier studies in this region (Jenny et al., 1949; Trumbore et al., 1996; Dahlgren et al., 1997; Rasmussen et al., 2006), we selected soils similar in age and vegetation along a combined gradient of parent material (granite, andesite, basalt) and MAT (12°C = "warm", 9°C = "cool", 5°C = "cold"). The climate gradient also represents a weathering gradient, with poorly developed soils at the cold climate sites, intermediately developed soils at the cool climate sites, and highly weathered soils at the warm climate sites (Harradine and Jenny, 1958; Rasmussen et al., 2010). Previous work at these sites confirmed strong differences in mineral assemblages along both the parent material and climate gradients, making these sites an ideal setting for probing the relative influence of climatic and mineralogical factors on soil C dynamics (Rasmussen et al., 2006; others?).

We were able to construct a time series of both $\Delta^{14}C_{bulk}$ and $\Delta^{14}C_{respired}$ at these sites by combining data from samples newly collected in 2019 with data from archived samples

116  collected in 2001 and 2009. Such a time series provides a crucial constraint for determining

117  the trajectory of bomb-derived $^{14}$C concentrations over time (Beem-Miller et al., 2020;

118  Stoner et al., 2020). Whether bomb-C concentrations are increasing or decreasing with time

119  depends on both on the distribution of soil C among pools with different cycling rates as well

120  as the year in which the soil was sampled, and thus cannot be easily determined from

121  observations at a single point in time (Baisden et al. 2003). Using the radiocarbon time

122  series in combination with previously determined mineralogical data, we were able to test

123  several hypotheses regarding the roles of mineralogical versus climatic factors in determining

124  both overall cycling rates and the dynamics of transiently cycling soil C.

125      We can expect soils with large stocks of persistent soil C to have depleted values of

126  $\Delta^{14}C_{bulk}$ relative to soils dominated by fast cycling soil C. If climate proves more important

127  than parent material for determining soil C persistence, than we would expect to see large

128  differences in $\Delta^{14}C_{bulk}$ among climate regimes when comparing soils within a given parent

129  material, but minimal differences among parent materials when comparing soils within the

130  same climate regime. However, if parent material proves more important than climate for

131  soil C persistence, we would expect the opposite trends in $\Delta^{14}C_{bulk}$: differences would be

132  greater among parent materials within a given climate regime than among climate regimes

133  within a given parent material. Alternatively, if persistent soil C is associated with specific

134  soil minerals, we would expect an interactive effect of parent material and climate on

135  $\Delta^{14}C_{bulk}$. For example, if soil C persistence is due to the association of soil organic matter

136  with poorly crystalline metal oxides, we would expect to observe the most depleted $\Delta^{14}C_{bulk}$

137  values where the combination of parent material and climate factors has led to the greatest

138  abundance of these specific soil minerals.

139      Soil C found in association with minerals is typically older than organic matter found

140  in free particulate forms [cite]. Accordingly, we might expect climate to be the dominant

141  factor controlling the amount and cycling rates of C in transiently cycling soil C pools, with

142 mineral factors being less relevant at these shorter timescales. If this hypothesis is correct,

143 we would expect to see greater differences in $\Delta^{14}C_{respired}$ among different climate regimes and

144 within a given parent material than we would among different parent materials within the

145 same climate regime. Furthermore, we would expect warmer climate soils to have $\Delta^{14}C_{respired}$

146 values closer to the atmosphere than colder climate soils, due to faster decomposition rates

147 in the actively cycling soil C pools, and accordingly, we would expect $\Delta^{14}C_{respired}$ to change

148 more over time at the warmer climate sites than at the colder climate sites.

# Methods

149

## Site descriptions

150

151    We collected samples from nine sites across a combined gradient of parent material and

152 climate in the Sierra Nevada Mountains of California (**Fig. 1**). Parent material changes

153 from basalt to andesite to granite along the north-south axis of the cordillera, while MAT

154 decreases as a function of increaing elevation along the east-west axis. Total mean annual

155 precipitation (MAP) ranges from 910 to 1400 mm yr$^{-1}$ across the sites. Precipitation

156 increases slightly with elevation (**Fig. 1**), and falls mainly as rain at lower elevations ($<$

157 1400 m), but mainly as snow at higher elevations ($>$ 1800 m). The andesitic and basaltic

158 parent materials receive slightly more precipitation on average than the granitic soils, with

159 MAP values of 1330 ($\pm$ 75) mm yr$^{-1}$, 1160 ($\pm$ 175) mm yr$^{-1}$, and 1000 ($\pm$ 85) mm yr-1 for

160 the andesite, basalt, and granite transects, respectively.

161    Vegetation at the study sites is typical of the Sierra Mixed Conifer habitat (Parker, I.,

162 and W. J. Matyas. 1981. CALVEG: a classification of Californian vegetation. U.S. Dep.

163 Agric., For. Serv., Reg. Ecol. Group, San Francisco). All of the sites are forested and

164 dominated by conifers, although the exact species composition changes along with climate.

165 Tree species at the lowest elevation warm climate sites are predominantly *Pinus ponderosa*

166 mixed with lesser amounts of *Quercus* spp. The canopy species at the mid-elevation cool

167 climate sites consist primarily of *Abies concolor* and *Pinus lambertiana*, while *Abies*

168 *magnifica* dominates at the high elevation cold climate sites. Species present at all sites

169 include *Calocedrus decurrens* in the canopy, the shrubs *Arctostaphylos* spp., *Chamaebatia*

170 *foliolosa*, and *Ceanothus* spp. in the understory, and patchy ground cover of grasses and

171 forbs (**Fig. 1**).

| Ecosystem | Dominant Vegetation | Elevation (m a.s.l.) | MAP (mm yr$^{-1}$) | MAT (°C) | Parent Material | Soil Taxonomy |
|---|---|---|---|---|---|---|
| PP | *Pinus ponderosa* | 920–1400 | 80–130 | 10–13 | GR | fine-loamy, mixed, semiactive, mesic Ultic Haploxeralf |
| | *Pinus lambertiana* | | Mostly rain | | BS | fine, kaolinitic, mesic Xeric Haplohumult |
| | *Quercus kelloggii* | | | | AN | fine, parasesquic, mesic Andic Palehumult |
| WF | *Abies concolor* | 1500–1800 | 80–130 | 8–10 | GR | coarse-loamy, mixed, superactive, mesic Humic Dystroxerept |
| | *Pinus ponderosa* | | Rain/snow | | BS | loamy-skeletal, mixed, superactive, mesic Typic Haploxerept |
| | *Pinus lambertiana* | | | | AN | medial-skeletal, amorphic, mesic Humic Haploxerand |
| RF | *Abies magnifica* | 2200–2400 | 100–130 | 5–6 | GR | mixed, superactive, frigid Dystric Xeropsamment |
| | *Pinus jeffreyi* | | snow | | BS | sandy-skeletal, mixed, superactive, frigid Typic Xerorthent |
| | | | | | AN | medial-skeletal, amorphic, frigid Humic Vitrixerand |

*Figure 1. NB: this is a placeholder—copied verbatim from Rasmussen et al. 2018* Dominant vegetation, climate parameters, and soil taxonomy for sampled ecosystems.[1] MAP—mean annual precipitation; MAT—Ecosystem abbreviations: PP—ponderosa pine; WF—white fir; RF—red fir. Dominant vegetation is listed in order of over-story dominance. Parent material abbreviations: GR—granite; BS—basalt; AN—andesite.

## Sample collection

173 Site locations were initially established in 2001 by C. Rasmussen (Rasmussen et al.,

174 2006), and resampled in 2009 (Rasmussen et al., 2018) and 2019 (this study). Three

175 replicate pits were dug to the depth of the B horizon (2001 sampling), or down to the C

176 horizon (2009 and 2019 sampling). Samples were collected from the pit sidewalls by horizon

177 in 2001 and 2009, and by 0.1 m increments in 2019. For the 2019 resampling, we located the

178 sites using GPS and geospatial coordinates recorded during site establishment. Prior to

179 sample collection we compared the soil profiles to the pedon descriptions from the 2001

180 sampling campaign to confirm the profiles matched. In 2019 we also measured the depth of

181 the litter layer and collected representative litter samples from each site. However, we only

182 focus on the upper mineral soil layers in this study (0 to ca. 0.3m) as the 2001 sampling was

183 restricted to this depth range.

## Incubations

185 Laboratory soil incubations were performed on composite samples from the three

186 replicate pedons sampled at each site in 2001 and 2019. We omitted the 2009 samples from

187 the incubation experiment to save on time and analysis costs, and because sample material

188 was only available from a single profile at each site. We composited and incubated each

189 depth increment separately in 1 L glass mason jars fitted with air tight sampling ports in the

190 lids. Incubations were performed in duplicate. Prior to the start of incubations we adjusted

191 the soil moisture content to 60% of water holding capacity (WHC). Samples from 2001 were

192 air-dried prior to archiving, and therefore we also air-dried the freshly collected soils from

193 2019 in order to control for the known effects of drying and rewetting on $\Delta^{14}C_{respired}$

194 (Beem-Miller et al., 2021). We defined WHC as the gravimetric water content of

195 water-saturated soil placed in mesh-covered (50µm) tubes (50ml) weighed after draining for

196 30 minutes on a bed of fine sand. Following rewetting we allowed the soils to respire for one

197 week before closing the jars. Incubations proceeded until $CO_2$ concentrations in the jar

198 headspace reached approximately 10,000 ppm, at which point we collected a 400 ml gas

199 subsample for radiocarbon analysis. Gas samples were collected with pre-evacuated

200 stainless-steel (Restec) vacuum canisters. All incubations were performed in the dark at

201 20°C.

**Soil Physical Analyses and Mineral Characterization**

Data on soil particle size distributions, bulk density, and mineral characterization were obtained from previously published analyses of samples collected at the study sites in 2001 and 2009 (Rasmussen et al. 2006, Rasmussen et al., 2018). Both qualitative and quantitative approaches were used to characterize soil mineral assemblages, including X-ray diffraction (XRD) for the clay (<2 µm) fraction, atomic absorption spectroscopy, and non-sequential selective dissolution. These previous analyses revealed that the dominant mineral species in the soils of the highly weathered warm climate zone were similar across parent materials, but differed substantially across parent materials at the less weathered cool and cold climate sites. Mineral assemblages at the warm climate sites are dominated by 1:1 clays and large accumulations of crystalline iron oxides [Dahlgren et al. 1997 "Soil development along an elevational transect in the western Sierra Nevada, California"; Rasmussen et al. 2007 "Soil Genesis and Mineral Transformation Across an Environmental Gradient on Andesitic Lahar"; Rasmussen et al. 2010 "Basalt weathering and pedogenesis across an environmental gradient in the southern Cascade Range, California, USA"]. In contrast, the cool and cold climate andesitic soils contain high concentrations of poorly crystalline short-range order (SRO) minerals such as allophane and iron oxyhydroxides. The cool and cold climate basaltic soils contain intermediate amounts of SRO minerals, while the granitic soils lack SRO minerals almost entirely, but are rich in quartz and contain relatively more hydroxyl-interlayered vermiculite than soils from the other lithologies.

The previous work at these sites showed that poorly crystalline metal oxide content was the best predictor of both C abundance and $\Delta^{14}C_{bulk}$. Accordingly, our analyses focus on the relationship between radiocarbon measurements and the abundance of poorly crystalline versus crystalline metal oxides as well as 2:1 versus 1:1 clays, but not the whole suite of mineralogical data. For simplification, we use the sum of ammonium-oxalate extractable aluminum and half of the ammonium-oxalate extractable Fe selectively dissolved

228 from bulk soils as a proxy for the abundance of poorly and non-crystalline metal oxides, and

229 the difference of dithionite-citrate extractable Fe and ammonium-oxalate extractable Fe for

230 the abundance of crystalline Fe in the main text. We present the results of additional

231 regression analyses looking at the specific relationships between $\Delta^{14}C_{bulk}$, $\Delta^{14}C_{respired}$, and

232 the concentration of Fe or Al extracted with ammonium-oxalate, Fe extracted with

233 dithionite-citrate, and Al extracted with sodium-pyrophosphate in the supplemental

234 information.

## Carbon, Nitrogen, and Radiocarbon Analysis

236 Total carbon and nitrogen content was determined by dry combustion (2019 samples:

237 Vario Max, Elementar Analysensysteme GmbH) on finely ground soils (2019 samples: Retch

238 MM400). For radiocarbon analysis of 2001 and 2019 samples, we first purified $CO_2$ from

239 combusted soil samples (bulk soils) and incubation flask samples (respired $CO_2$) on a

240 vacuum line using liquid $N_2$. Following purification, samples were graphitized with an iron

241 catalyst under an $H_2$ enriched atmosphere at 550°C. Radiocarbon content was then

242 measured by accelerator mass spectrometry (Micadas, Ionplus, Switzerland) at the Max

243 Planck Institute for Biogeochemisty (Steinhof, 2017). See Rasmussen et al. (2018) for details

244 of C, N, and radiocarbon analysis of the 2009 samples.

245 We report radiocarbon values using units of $\Delta^{14}C$, defined as the deviation in parts per

246 thousand of the ratio of $^{14}C$–$^{12}C$ from that of the oxalic acid standard measured in 1950.

247 This unit also contains a correction for the potential effect of mass-dependent fractionation

248 by normalizing sample $\delta^{13}C$ to a common $\delta^{13}C$ value of -25 per mil (Stuiver & Polach, 1977).

249 Values with $\Delta^{14}C > 0$ indicate the presence of "bomb" C produced by atmospheric weapons

250 testing in the early 1960s. Values with $\Delta^{14}C < 0$ indicate the influence of radioactive decay

251 of $^{14}C$, which has a half-life of 5730 years.

**Spline fitting**

We used a spline function to compare soil properties from samples collected from different depth intervals in different years and at different sites. We were motivated to use consistent depth increments across sites when resampling in 2019 because of the strong correlation between depth and $\Delta^{14}$C observed in the 2009 dataset, a correlation also noted in numerous other studies (Mathieu et al., 2015; Shi et al., 2020; others...). We fit a mass-preserving quadratic spline to the 2001 and 2009 profiles in order to convert soil property data to the equivalent depth increments sampled in 2019 (Bishop et al., 2001). We performed the spline fitting with the mpspline function of the GSIF package in R, using a $\lambda$ value of 0.1 (Hengl 2019).

**Statistical analysis**

We used a linear modeling approach to assess the relative explanatory power of climate versus parent material on the observed variation in $\Delta^{14}$C, as well as potential interactions between these two factors. We constructed separate models for $\Delta^{14}$C$_{bulk}$ and $\Delta^{14}$C$_{respired}$ but with the same equation structure (Eq. 1). For each model we considered the two-way interaction between parent material and climate as well as the three-way interaction with time (**Eq. 1**). For ease of interpretation, we considered the effect of depth by modeling each depth layer separately (0-10 cm, 10-20 cm, 20-30 cm). We also made pairwise comparisons of $\Delta^{14}$C$_{bulk}$ and $\Delta^{14}$C$_{respired}$ across sites and within years, and across years for individual sites. We assessed the significance of the temporal trend for pairwise combinations of parent material and climate using the emmtrends function of the emmeans package (Lenth, 2021). We corrected for multiple comparisons using Tukey's honestly significant mean difference.

**Eq. 1**

$$\Delta^{14}C = \alpha + \beta_1(Parent\_material) \times \beta_2(Climate) \times \beta_3(Year) + \varepsilon$$

Where $\alpha$ is the intercept term, the $\beta$ terms are coefficients, and $\varepsilon$ is random error.

276    We also considered the relationship between $\Delta^{14}C_{bulk}$ and $\Delta^{14}C_{respired}$ to gain insight

277  into potential differences in soil C dynamics and persistence mechanisms across our sites

278  (Sierra et al. 2018). We modeled the effects of parent material (**Eq. 2**) and climate (**Eq. 3**)

279  on this relationship separately, as we did not have an adequate number of observations to

280  consider the interaction between these two explanatory variables. For this analysis we used

281  $\Delta^{14}C$ measurements made on samples collected in 2001 and 2019, and data from all depths.

282  The three-way interactions of $\Delta^{14}C_{bulk}$ and the explanatory variables (parent material or

283  climate) were not significant with either depth or time for either **Eq. 2** or **Eq. 3**, so we did

284  not include either depth or time as variables in the models.

285    **Eq. 2**

$$\Delta^{14}C_{respired} = \alpha + \beta_1(\Delta^{14}C_{bulk}) \times \beta_2(Parent\_material) + \epsilon$$

286    **Eq. 3**

$$\Delta^{14}C_{respired} = \alpha + \beta_1(\Delta^{14}C_{bulk}) \times \beta_2(Climate) + \epsilon$$

287    We assessed the relative importance of poorly crystalline versus crystalline iron

288  minerals in protecting soil C from microbial decomposition by regressing $\Delta^{14}C$ against the

289  concentrations of ammonium-oxalate extractable iron, ammonium-oxalate extractable

290  aluminum, pyrophosphate extractable aluminum, and dithionite-citrate extractable iron (**Eq.**

291  **4**). We fit the model for $\Delta^{14}C_{bulk}$, $\Delta^{14}C_{respired}$, and the difference between $\Delta^{14}C_{respired}$ and

292  $\Delta^{14}C_{bulk}$ ($\Delta^{14}C_{bulk\text{-}respired}$). We used $\Delta^{14}C$ data from 2001, 2009, and 2019 for the $\Delta^{14}C_{bulk}$

293  model, but only data from 2001 and 2019 for the $\Delta^{14}C_{respired}$ and $\Delta^{14}C_{bulk\text{-}respired}$ models.

294  Selective dissolution was only performed on the soils collected in 2001, but these data were

295  assumed to be comparable for the other time points as they reflect weathering processes

296  operating at timescales beyond the 18-year duration of this study. The regression analysis

297  conducted with **Eq. 4** was done for the combined depth increment of 0 to 0.3 m, as

298  extracted metal concentrations did not change substantially over this increment. Combining

depth increments allowed us to control for the depth dependence of $\Delta^{14}$C as well as simplify interpretation of the data. In order to obtain values for the necessary data over the 0 to 0.3 m depth increment we computed mass-weighted estimates of extractable metal concentrations, carbon mass-weighted means of $\Delta^{14}$C$_{bulk}$ and flux-weighted means of $\Delta^{14}$C$_{respired}$; these calculations were made prior to determining $\Delta^{14}$C$_{bulk\text{-}respired}$.

**Eq. 4**

$$\Delta^{14}C = \alpha + \beta_1(Metal_x) + \beta_2(time) + \varepsilon$$

Where $\alpha$ is the intercept term, $\beta$ is the coefficient for each factor in the model, $Metal_x$ is the concentration of selectively dissolved metal oxides, time is the year of sampling, and $\varepsilon$ is random error.

## Results

### Soil carbon concentrations and flux rates

We observed both parent material and climate effects on soil organic C (SOC) concentration. SOC concentrations were similar among parent materials for the warm climate sites (**Fig. 2, a**), while at the cool and cold climate sites (**Fig. 2, b, c**) the andesitic soils had higher SOC concentrations than either the basaltic or granitic soils. The basaltic and granitic soils had similar SOC concentrations across climate zones, while the cool and cold climate andesitic soils were enriched in C relative to the warm climate soils. Soils showed a similar decrease in SOC concentration with depth across all sites (**Fig. 2**).

We did not observe significant changes in SOC concentration over time for the majority of our sites. We saw the most substantial variation in SOC concentration between 2001, 2009, and 2019 in the surface layers (0-0.1 m), with significant differences observed between years for the warm climate andesitic and basaltic sites, and for the deeper (0.1-0.2 m, 0.2-0.3 m) depth layers at the cold climate andesitc site (**SI Fig. 1**). We observed similar trends in

322  SOC stocks across sites as with SOC concentration, despite lower bulk densities in the

323  andesitic sites with high C concentrations (**SI Fig. 2**). However, we did not assess soil

324  carbon stock changes over time in this study as we did not measure bulk density in 2019,

325  and earlier sampling campaigns did not incorporate adequate spatial replication for making

326  such an assessment (Johnson et al., 1990; Schrumpf et al., 2013).

327  Flux rates of heterotrophic respiration differed among parent materials and among

328  climate zones. When compared on a carbon basis (mg $CO_2$ g $C^{-1}$ $d^{-1}$), flux rates tended to

329  be higher for the andesitic soils than soils from either basaltic or andesitic soils, particularly

330  at depth (**SI Fig. 2**). The exceptions to this trend were the surface (0-0.1 m, 2001 and

331  2019) and near-surface (0.1-0.2 m, 2019) soils from the warm climate sites (**SI Fig. 2**).

332  Respiration rates for granitic and basaltic soils tended to decrease with decreasing MAT

333  (warm > cool > cold); however, we did not see any clear trend in respiration rates with

334  respect to climate for the andesitic soils (**SI Fig. 2**).

## Radiocarbon depth profiles

336  **Bulk soil.** $\Delta^{14}C_{bulk}$ covaried with both parent material and climate. We observed

337  the most enriched $\Delta^{14}C_{bulk}$ at the warm climate sites, indicating a preponderance of

338  relatively young, fast-cycling C. However, contrary to what would be expected from the

339  decomposition-temperature relationship, we observed the oldest soil C (i.e. most depleted

340  $\Delta^{14}C_{bulk}$ values) at the intermediate MAT cool climate sites rather than at the cold climate

341  sites (**Fig. 3, b, c**) (**Fig. 3, a**). When comparing $\Delta^{14}C_{bulk}$ from different parent materials

342  within a given climate zone, $\Delta^{14}C_{bulk}$ of andesitic soils tended to be the most depleted, while

343  the granitic soils tended to be the most enriched (**Fig. 3**). We focus on the 2019 data here

344  for simplicity, but $\Delta^{14}C_{bulk}$ profiles showed similar patterns in both 2001 (**SI Fig. 2**) and

345  2009 (Rasmussen et al., 2018).

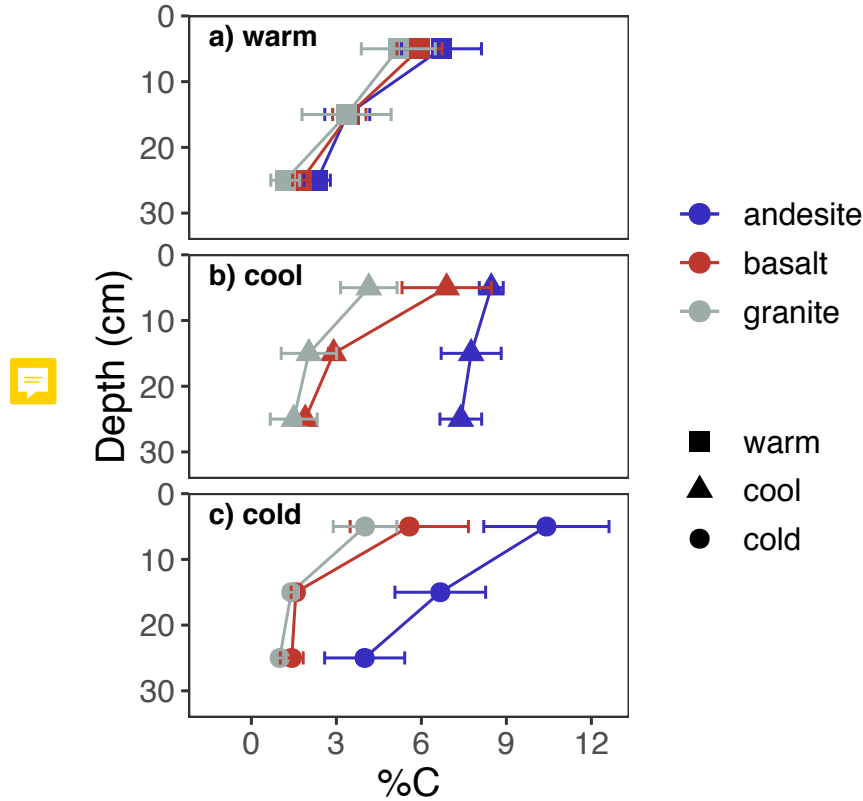346  Analysis of variance for $\Delta^{14}C_{bulk}$ revealed significant two-way interactions between

*Figure 2*. Profiles of soil C concentration. Points show mean of 2001, 2009, and 2019 data; error bars show $\pm$2SE.

parent material and climate at all depths (**Table 1**). This interaction was evident in the differences in $\Delta^{14}C_{bulk}$ that we observed among parent materials within each climate zone. We observed the greatest differences in $\Delta^{14}C_{bulk}$ among parent materials at the warm and cool sites (**Fig. 3, a, b**), while $\Delta^{14}C_{bulk}$ was similar among parent materials at the coldest sites (**Fig. 3, c**). We also found depth to be an important factor influencing the relative importance of climate versus parent material effects on $\Delta^{14}C_{bulk}$. Although $\Delta^{14}C_{bulk}$ declined with depth for all sites, climate explained more of the variance in $\Delta^{14}C_{bulk}$ in the uppermost soil layer (0-10 cm) whereas parent material explained more in the bottom two layers (10-20 cm, 20-30 cm) (**Table 1**).

**Heterotrophically respired CO$_2$.** The patterns we observed in $\Delta^{14}C_{respired}$ were similar to those we observed in $\Delta^{14}C_{bulk}$ (**Fig. 3**). We found climate to the only significant

358 factor for explaining the variance observed in $\Delta^{14}C_{respired}$ in the uppermost soil layer (0-0.1

359 m), while at the deepest depth (0.2-0.3 m) parent material was more important than climate

360 (**Table 1**). Overall, we found the two-way interaction between parent material and climate

361 explained more of the variance in $\Delta^{14}C_{respired}$ than it did in $\Delta^{14}C_{bulk}$ (**Table 1, *F* values**).

362      The effect of climate on $\Delta^{14}C_{respired}$ appeared to be moderated by parent material.

363 Accordingly, we did not observe significant differences in $\Delta^{14}C_{respired}$ among the andesitic

364 soils when compared across climate zones at any depth (SI Table XX Tukey results for emm).

365 In contrast, $\Delta^{14}C_{respired}$ diverged substantially between climate zones for the basaltic and

366 granitic soils, particularly for the 0.1-0.2 m and 0.2-0.3 m depth layers (**Fig. 3**). Overall,

367 $\Delta^{14}C_{respired}$ values across sites were most similar at the soil surface (0-0.1 m), and most

368 divergent at the intermediate depth (0.1-0.2 m) (**Fig. 3**).

369 **Radiocarbon time series**

370      Temporal trends in bulk and respired $\Delta^{14}C$ reflect the degree to which soil C is

371 exchanging with C fixed from the atmosphere. The average annual decline in $\Delta^{14}C$

372 atmospheric $CO_2$ between 2001 and 2009 for the northern hemisphere was -5.13 per mille

373 yr$^{-1}$ (Graven et al., 2017; Sierra, 2018) (**Fig. 4, dotted lines**). Therefore, changes in $\Delta^{14}C$

374 of soil C that parallel the atmospheric trend must be exchanging relatively rapidly compared
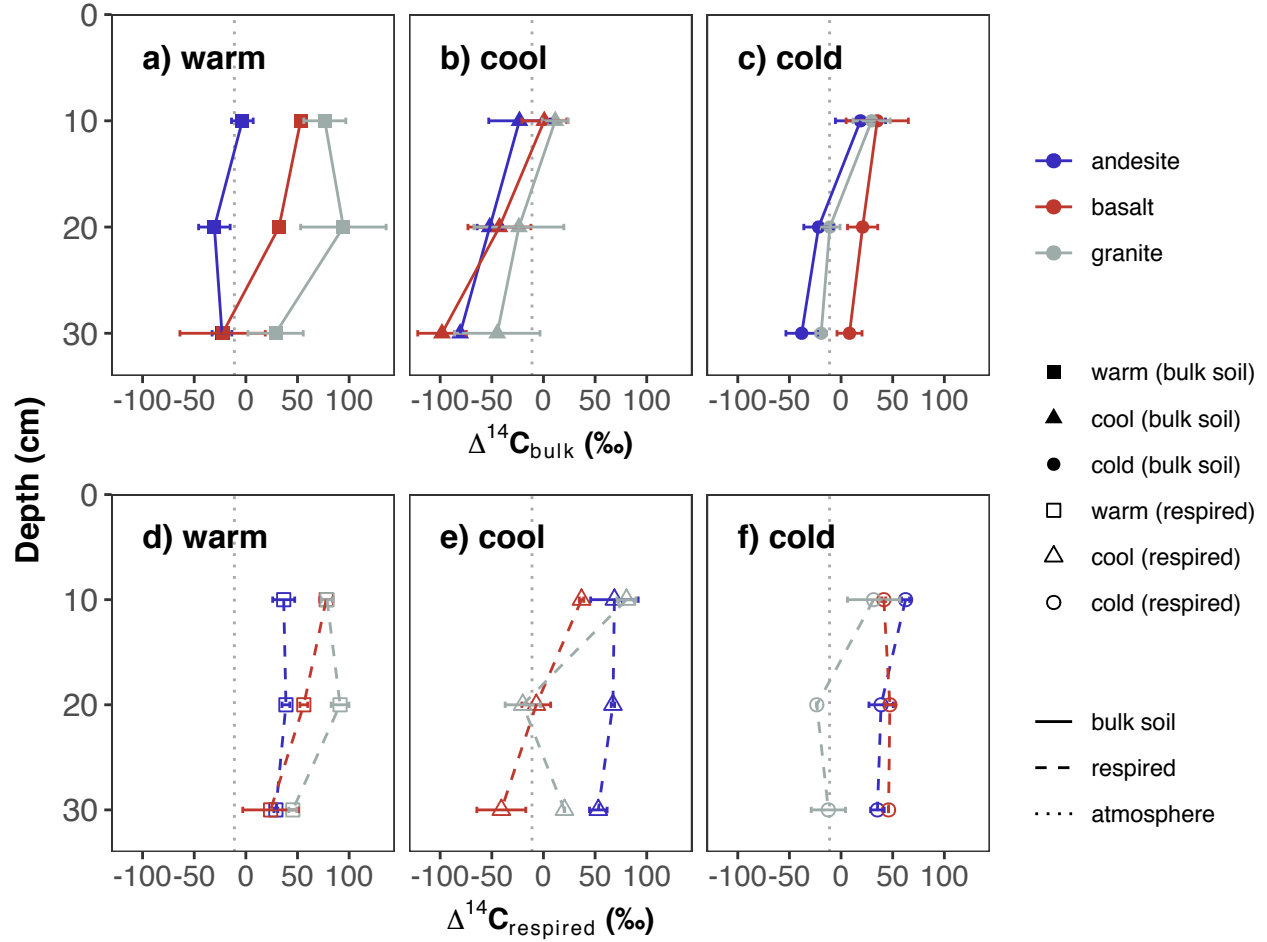
375 to those that change little over the same time period.

*Figure 3*. Depth profiles of $\Delta^{14}C_{bulk}$ and $\Delta^{14}C_{respired}$ in 2019. Top panels show bulk data, bottom panels show respired data. Panels (a) and (d) show data from the warm climate sites, (b) and (e) from the cool climate sites, and (c) and (f) from the cold climate sites. Black vertical lines show $\Delta^{14}C$ of the atmosphere in 2019. Points show the mean of three replicate profiles for bulk soil, and the mean of laboratory duplicates for respired $CO_2$. Error bars show $\pm 1$ SD for bulk soils and the minimum and maximum for respired $CO_2$.
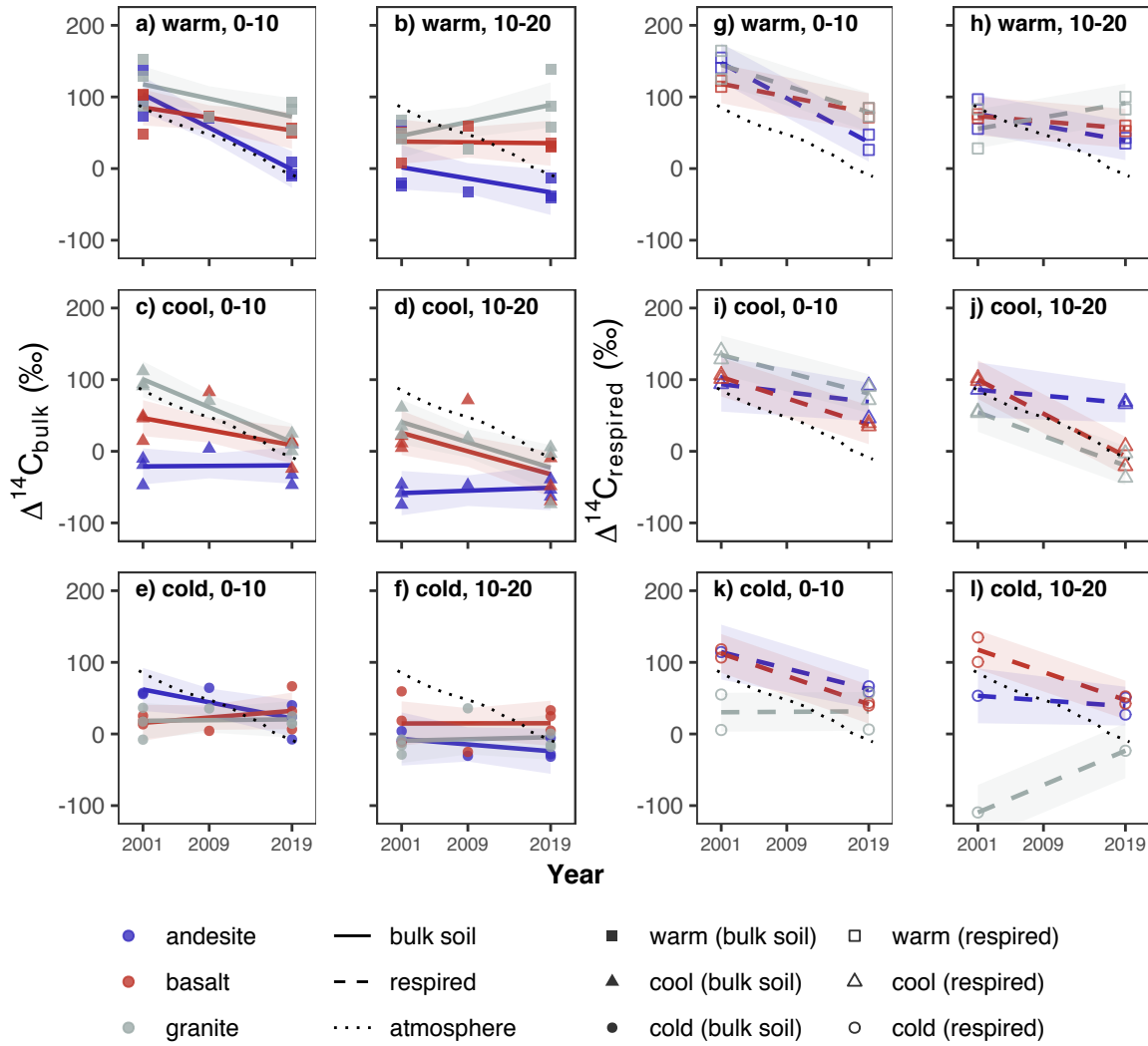
*Figure 4.* Temporal trends in $\Delta^{14}$C for 0-10 cm and 10-20 cm depth layers. Panels a-f show $\Delta^{14}$C$_{bulk}$ data; from left, the first column (panels a, c, and e) show 0-10 cm data, and the second column (panels b, d, and f) shows 10-20 cm data. Panels g-l show $\Delta^{14}$C$_{respired}$ data; the third column from left (panels g, i, k) shows 0-10 cm data, and the rightmost column (panels h, j, and l) shows 10-20 cm data. Points show observed data; lines show linear trend estimates for marginal means; ribbons show 95% confidence intervals for trends. Dotted line shows atmospheric $\Delta^{14}$C.

Table 1

*ANOVA for $\Delta^{14}C_{\text{bulk}}$ and $\Delta^{14}C_{\text{respired}}$*

| Depth | Predictor | Bulk soil | | | Respiration | | |
|---|---|---|---|---|---|---|---|
| | | *df* | *F* | *p* | *df* | *F* | *p* |
| 0-10cm | Parent material | 2 | 12.00 | **< .001** | 2 | 0.04 | 0.958 |
| | Climate | 2 | 32.34 | **< .001** | 2 | 14.02 | **< .001** |
| | Year | 1 | 32.03 | **< .001** | 1 | 75.29 | **< .001** |
| | Parent material:Climate | 4 | 8.75 | **< .001** | 4 | 7.90 | **0.001** |
| | Parent material:Year | 2 | 2.38 | 0.105 | 2 | 1.93 | 0.177 |
| | Climate:Year | 2 | 6.61 | **0.003** | 2 | 2.26 | 0.137 |
| | Parent material:Climate:Year | 4 | 5.19 | **0.002** | 4 | 3.75 | **0.024** |
| | Residuals | 44 | | | 16 | | |
| 20-30cm | Parent material | 2 | 15.58 | **< .001** | 2 | 0.92 | 0.421 |
| | Climate | 2 | 11.61 | **< .001** | 2 | 0.77 | 0.483 |
| | Year | 1 | 1.30 | 0.26 | 1 | 0.65 | 0.434 |
| | Parent material:Climate | 4 | 1.71 | 0.165 | 4 | 4.33 | **0.019** |
| | Parent material:Year | 2 | 1.56 | 0.222 | 2 | 0.86 | 0.446 |
| | Climate:Year | 2 | 4.04 | **0.024** | 2 | 1.41 | 0.278 |
| | Parent material:Climate:Year | 4 | 0.98 | 0.43 | 2 | 0.37 | 0.698 |
| | Residuals | 44 | | | 13 | | |

376      **Bulk soil.** We observed a significant three-way interaction between parent material,

377 climate, and time at all three depths in the linear models (**Eq. 1**) for $\Delta^{14}C_{bulk}$ (**Table 1**).

378 The change over time in $\Delta^{14}C_{bulk}$ was also affected by depth, with greater differences seen

379 between 2001 and 2019 in the uppermost soil layer than in the deeper layers (**Fig. 4**). We

380 observed a significant decrease in $\Delta^{14}C_{bulk}$ over time in both warm and cool climate granitic

381 soils for the uppermost soil layer (0-0.1 m), and additionally for the warm climate andesitic

382 soils (**Fig. 4, a**). In the deeper soil layers (0.1-0.2 m and 0.2-0.3 m), we only observed a

383 significant change over time in $\Delta^{14}C_{bulk}$ for the cool climate basalt and granite soils (**Fig. 4,**

384  **c, d**, 0.2-0.3 m data not shown). $\Delta^{14}C_{bulk}$ of the cool climate andesitic soils remained

385  essentially unchanged between 2001 and 2019 for all depths (**Fig. 4, c, d**, 0.2-0.3 m data

386  not shown), underscoring the importance of the interaction between parent material and

387  climate for explaining temporal trends in $\Delta^{14}C_{bulk}$.

388      The relationship of $\Delta^{14}C_{bulk}$ to atmospheric $\Delta^{14}C$ also depended on the combination of

389  parent material and climate. In 2001, the warm climate sites were the only sites where the

390  basaltic and andesitic soils were enriched relative to the atmosphere, and this enrichment

391  was only observed for the uppermost soil layer (**Fig. 4)**). In contrast, granitic soils at both

392  the warm and cool climate sites were enriched relative to the atmosphere in 2001 (**Fig. 4**).

393  For the cold climate sites, where $\Delta^{14}C_{bulk}$ was most similar, all three lithologies were

394  depleted relative to atmospheric in both surface and subsoil layers in 2001 (**Fig. 4, e, f**).

395      We observed that $\Delta^{14}C_{bulk}$ tended to decrease or remain unchanged between 2001 and

396  2019 across sites, but the rates of change in $\Delta^{14}C_{bulk}$ were typically smaller than the

397  corresponding change in atmospheric $\Delta^{14}C$ over the same period. Accordingly, $\Delta^{14}C_{bulk}$

398  measured in 2019 tended to be enriched relative to the atmosphere at more sites, and also

399  more enriched at depth than in 2001. We observed surface soil $\Delta^{14}C_{bulk}$ (0-0.1 m) in 2019 to

400  be enriched relative to the atmosphere at all sites except for the cool climate andesite soils

401  (**Fig. 4; Fig. 3, d-f**). Furthermore, $\Delta^{14}C_{bulk}$ was enriched relative to the atmosphere down

402  to 30 cm at two of the sites in 2019: the warm climate granite soil (**Fig. 3, d**) and cold

403  climate basalt soil (**Fig. 3, f**). $\Delta^{14}C_{bulk}$ at the cool climate andesite site was the most

404  depleted relative to the atmosphere at all time points (**Fig. 4**).

405      **Heterotrophically respired CO$_2$.**  Temporal trends in $\Delta^{14}C_{respired}$ tended to be of

406  greater magnitude than what we observed for $\Delta^{14}C_{bulk}$ (**Fig. 4, g-l**). However, changes in

407  $\Delta^{14}C_{respired}$ between 2001 and 2019 still tended to be smaller in magnitude than the change

408  observed in the atmosphere over this period (**Fig. 4, g-l**). In contrast to $\Delta^{14}C_{bulk}$,

409  $\Delta^{14}C_{respired}$ values of both surface and near surface soils (0-0.2 m) were close to atmospheric

410 levels in 2001, while in 2019, $\Delta^{14}C_{respired}$ tended to be enriched relative to the atmosphere,

411 even for the deeper soil layers (**Fig. 4, g-l**).

412 We saw significant decreases in $\Delta^{14}C_{respired}$ values of surface (0-0.1 m) soils at seven of

413 the nine sites, with the only exceptions being the cool climate andesitic and cold climate

414 granitic sites (**Fig. 4, g-l**). In absolute terms, the changes in $\Delta^{14}C_{respired}$ over time in the

415 uppermost soil layer were greatest at the warm sites (-4 $\pm$2 per mil yr$^{-1}$), while changes were

416 similar for the cool and cold sites (-2.7 $\pm$1.2 per mil yr$^{-1}$, and -2.2 $\pm$2.1 per mil yr$^{-1}$,

417 respectively). When considered within parent materials, granitic soils showed the greatest

418 decrease in $\Delta^{14}C_{respired}$ over time at the warm climate site and the least change at the cold

419 climate site. In contrast, the andesitic soils showed the least amount of change over time at

420 the cool climate sites, while changes over time in the basaltic soils were similar across all

421 three climate regimes. The magnitude of the change in $\Delta^{14}C_{respired}$ over time tended to

422 decrease with depth for all soils. We observed significant negative trends over time for

423 $\Delta^{14}C_{respired}$ at only four of the nine sites for the 0.1-0.2 m layer (warm andesite, cool basalt,

424 cool granite, and cold basalt) (**Fig. 4**), and only one site for the 0.2-0.3 m layer (cold basalt)

425 (SI Fig. XX). $\Delta^{14}C_{respired}$ at the cool andesitic soils remained unchanged at all depths over

426 the study period.

427 We observed a significant increase in $\Delta^{14}C_{respired}$ from 2001 to 2019 at only one site:

428 the cold climate granitic soil (**Fig. 4**). This was also the only soil for which $\Delta^{14}C_{respired}$ was

429 more depleted than $\Delta^{14}C_{bulk}$. We observed this anomaly for the deeper soil layers in both

430 2001 and 2019. We observed $\Delta^{14}C_{respired}$ values of -469.1-127.8 per mil for the 8-27 cm layer

431 in 2001, compared to $\Delta^{14}C_{bulk}$ values between -30.80 and -10.50. Similarly, we observed

432 $\Delta^{14}C_{respired}$ values of -396.70 and -23.50 per mil for the 10-20 cm layer in 2019, compared to

433 -18.10 and 0.40 for $\Delta^{14}C_{bulk}$ (SI Table X). However, since these anomalous values of

434 $\Delta^{14}C_{respired}$ were restricted to the deeper soil layers from this one site, and were consistent

435 over time, the response appears to be a laboratory artifact unique to these soils. Accordingly,

436 we have excluded these highly depleted samples from the statistical analyses.

## Relationship of bulk soil and respired $CO_2$ $\Delta^{14}C$

438     We assessed the relationship between $\Delta^{14}C_{bulk}$ and $\Delta^{14}C_{respired}$ using linear regression
439 models for parent material (**Eq. 3**) and climate (**Eq. 4**). We observed $\Delta^{14}C_{respired}$ to be
440 enriched relative to $\Delta^{14}C_{bulk}$ for almost all sites and all depths, but that the magnitude of
441 the difference depended on both parent material and climate. Accordingly, y-intercepts for
442 all models were equal to or greater than zero, indicating that respired $CO_2$ in these soils is
443 predominantly modern (i.e. $< 60$ years old) for all but the deepest soil layers, regardless of
444 parent material or climate regime. We found the largest y-intercept values for the soils
445 developed on andesitic parent material, and for soils in the cool climate zones, which
446 indicates that $CO_2$ respired from these soils is relatively enriched in decadally cycling
447 bomb-C.

448     Slope values less than 1 in these models indicate that every per mille change in
449 $\Delta^{14}C_{bulk}$ is associated with a correspondingly smaller change in $\Delta^{14}C_{respired}$. This suggests
450 that the process regulating persistence of soil C on long time scales is distinct from that
451 which regulates more transiently cycling soil C. Similar to what we found for the
452 y-intercepts, modeled slopes for the parent material-only model (**Eq. 2**) were smallest for
453 the andesitic soils (slope $= 0.51$, 95% CI $= [0.22, 0.80]$) (**Fig. 5, a**), and for cool climate
454 soils in the climate-only model (**Eq. 3**) (slope $= 0.61$, 95% CI $= [0.30, 0.91]$) (**Fig. 5, b**).
455 While we could not directly test the interaction of parent material and climate factors in
456 these models owing to the limited number of observations, we observed that mean differences
457 in $\Delta^{14}C_{bulk}$ and $\Delta^{14}C_{respired}$ were substantially greater for the cool climate soils developed on
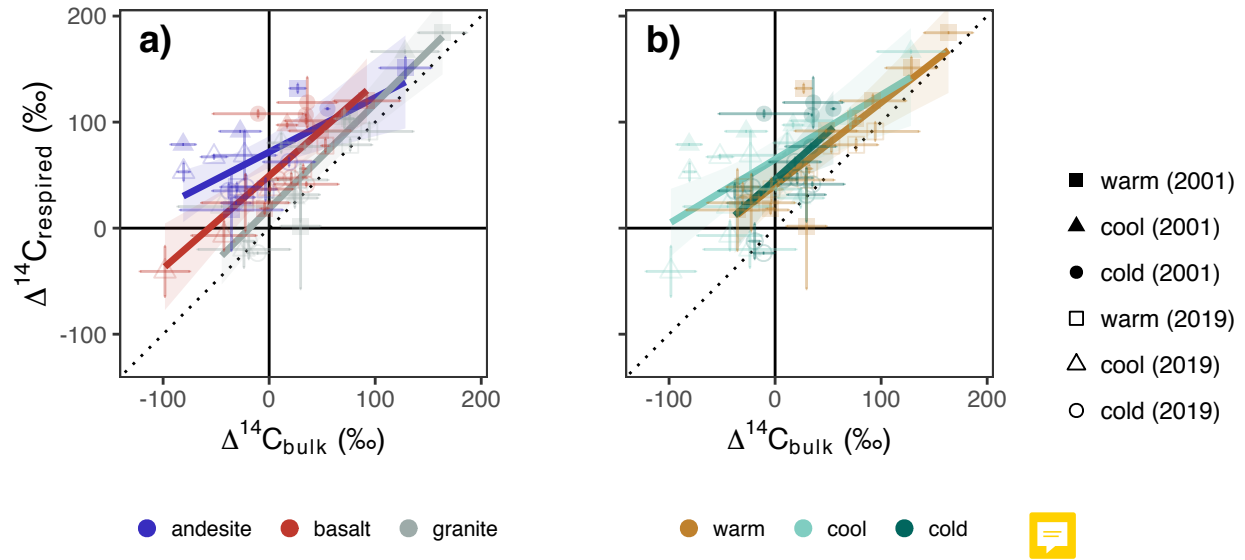458 andesitic parent material than for the other sites.

*Figure 5*. Parent material and climate effects on the relationship of $\Delta^{14}C_{bulk}$ and $\Delta^{14}C_{respired}$. [a)] Parent material model **(Eq. 3)** and [b)] Climate model **(Eq. 4)**. Dotted line shows 1:1 relationship. Points show the mean of three replicate profiles for bulk soil, and the mean of laboratory duplicates for respired $CO_2$. Error bars show $\pm 1$ SD for bulk soils and the minimum and maximum for respired $CO_2$. Respired $CO_2$ from the cold granite site in 2001 was extremely depleted in $\Delta^{14}C$ and thus is excluded for display purposes.

**Mineral assemblages and radiocarbon**

Mineral assemblage data is reported fully in Rasmussen et al. (2018). Here we focus on the selective dissolution data with respect to the trends we observed in $\Delta^{14}C_{bulk}$, $\Delta^{14}C_{respired}$, and $\Delta^{14}C_{respired\text{-}bulk}$. We observed a significant negative correlation between $\Delta^{14}C_{bulk}$ and the concentration of oxalate extractable iron, oxalate extractable aluminum, and pyrophosphate extractable aluminum (SI). For simplicity, we focus here on the sum of oxalate extractable aluminum and half of the oxalate extractable iron as a proxy for non-crystalline metal oxide abundance, and the difference of dithionite-citrate extractable iron and ammonium-oxalate extractable iron as a proxy for crystalline Fe-oxide abundance. The relationship between non-crystalline oxide abundance and $\Delta^{14}C_{bulk}$ was highly significant ($p <0.001$), with the model explaining 0 percent of the observed variation. In contrast, we did not find a significant relationship between crystalline Fe-oxide abundance and $\Delta^{14}C_{bulk}$.

We observed a relationship between $\Delta^{14}C_{respired}$ and poorly crystalline metal oxide abundance that was significant at $\alpha = 0.1$, but not at $\alpha = 0.05$ ($p = 0.07$). The marginal significance of this relationship is not surprising given that this regression considered flux-weighted means, and the majority of the $CO_2$ flux came from the 0-0.1 m soil layer where climate was the dominant control on $\Delta^{14}C_{respired}$. However, we did see a highly significant relationship between poorly crystalline metal oxide abundance and $\Delta^{14}C_{respired\text{-}bulk}$ (**Fig. 6, a**). As with $\Delta^{14}C_{bulk}$, there was no relationship with crystalline Fe-oxide abundance for either $\Delta^{14}C_{respired}$ or $\Delta^{14}C_{respired\text{-}bulk}$ (**Fig. 6, b**).

## Discussion

Climatic and mineralogical factors both play key roles in soil carbon persistence. However, the relevance of parent material for explaining soil organic matter persistence in soils with mixed mineralogies is still poorly explained. In the current study we illuminate how parent material interactions with climate lead to the development of distinct mineral assemblages, which in turn control the dynamics of soil C cycling at timescales ranging from
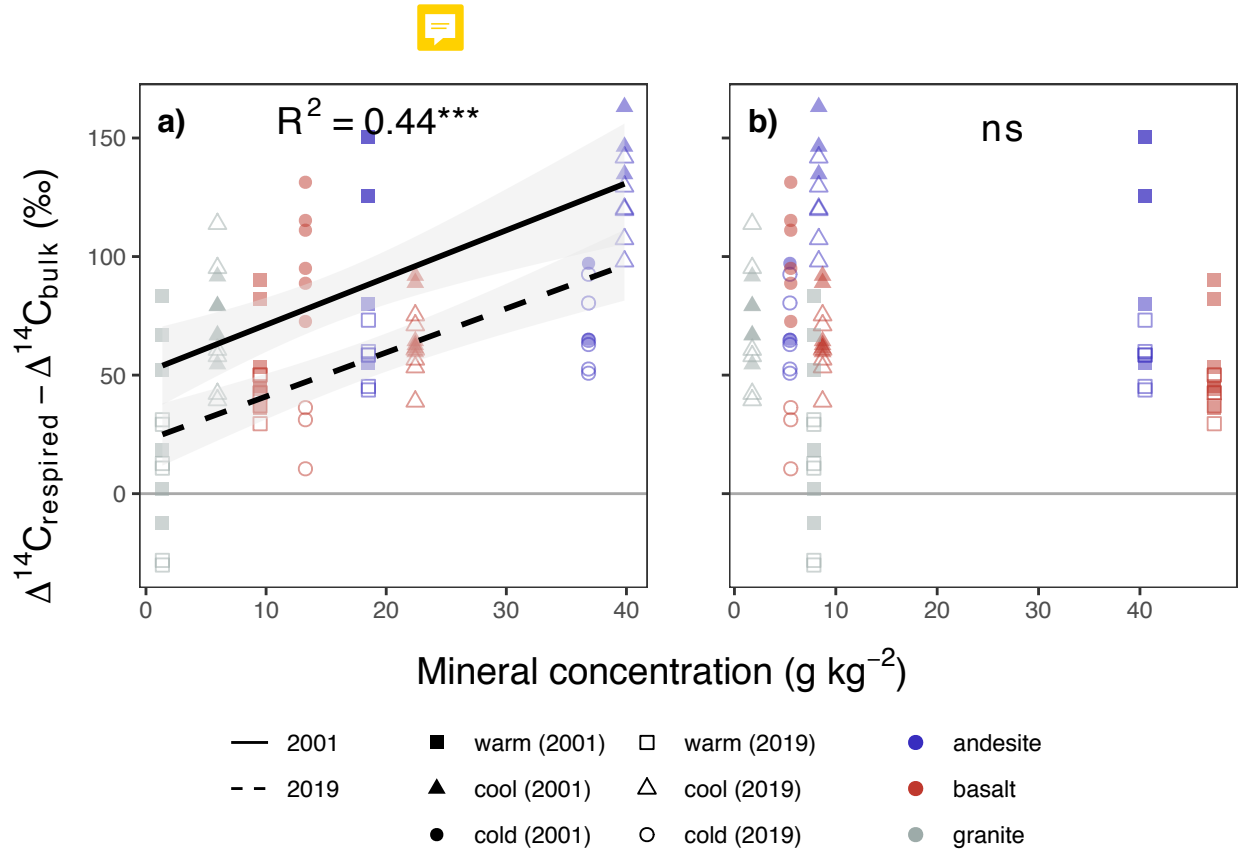
*Figure 6*. Relationship of poorly crystalline and crystalline minerals to the difference of $\Delta^{14}C_{respired}$ and $\Delta^{14}C_{bulk}$ ($\Delta^{14}C_{respired-bulk}$). [a)] Poorly crystalline metal oxide content (oxalate-extractable aluminum + 1/2 oxalate-extractable iron), [b)] Crystalline Fe content (dithionite-extractable iron - oxalate-extractable iron). Points show mass-weighted mineral concentrations and carbon-weighted values of $\Delta^{14}C_{respired-bulk}$ for 0-30cm profiles. Lines show linear model fits from **Eq. 5**.

annual to centennial. Our key findings are that soil mineral characteristics mediate climatic controls on soil C cycling, and that mineralogical controls on soil C cycling are not limited to soil C persistence on centennial timescales, but are relevant for C cycling on shorter timescales as well.

Our results challenge the primacy of climatic controls on soil carbon persistence, insofar as we observed the most depleted $\Delta^{14}C_{bulk}$ in soils of the cool climate zone, not the cold climate zone. We found that climate is a critical factor for explaining the dynamics of both persistent and more transient soil C pools, as measured by proxy with $\Delta^{14}C_{bulk}$ and $\Delta^{14}C_{respired}$, respectively. However, our results indicate that soil mineral characteristics moderate the strength of the climate effect. This is particularly apparent at depth. These results are supported by a recent study in which the authors used a depth-resolved model with energy and substrate limitation prescribed by Michalis Menten kinetics to model profiles of $\Delta^{14}C_{bulk}$ (Ahrens et al. 2020). The authors found that site mean annual temperature could only explain a minimal amount of variation in the observed radiocarbon profiles, while varying sorption potential in the model allowed for a superior fit.

Previous work at our study sites showed that poorly crystalline metal oxides were key to explaining both soil C accumulation and $\Delta^{14}C_{bulk}$ values in these soils (Rasmussen et al., 2018). Our results confirm these findings and extend them to demonstrate a significant correlation between poorly crystalline metal oxide abundance and $\Delta^{14}C_{respired\text{-}bulk}$ and a marginally significant correlation with $\Delta^{14}C_{respired}$. We focus here on $\Delta^{14}C_{respired\text{-}bulk}$, as this metric offers a unique insight into the magnitude of the difference between the cycling rates of persistent and more transiently cycling soil C.

We would expect the greatest differences between $\Delta^{14}C_{respired}$ and $\Delta^{14}C_{bulk}$ to be found in soils with a pool of old soil C protected from decomposition in some way, and another pool of soil C that is readily decomposed. In contrast, the smallest differences should occur for soils lacking strong soil C protection mechanisms, in which the majority of soil C has an

equal probability of being decomposed by microbes. Accordingly, we observed the smallest differences between $\Delta^{14}C_{respired}$ and $\Delta^{14}C_{bulk}$ in the soils with the lowest concentration of poorly crystalline metal oxides, while we observed the largest differences in the soils with the highest concentrations of these minerals. We interpret these findings as providing evidence for a key role of poorly crystalline metal oxides in protecting soil organic matter from decomposition. The values of $\Delta^{14}C_{bulk}$ in the subsurface layers (0.1-0.3 m) of the soils with low poorly crystalline metal oxide content (e.g. granitic soils) were depleted relative to the atmosphere, indicating persistent soil C, but we also observed similarly depleted values of $\Delta^{14}C_{respired}$ in these soils. This suggests that soil C persistence in these soils is due to other physical constraints on decomposition that are alleviated under laboratory incubation conditions, for example transport or isolation [Gleixner et al., 2013].

The soils with the largest difference between $\Delta^{14}C_{respired}$ and $\Delta^{14}C_{bulk}$ were those that had both strongly depleted values of $\Delta^{14}C_{bulk}$ and values of $\Delta^{14}C_{respired}$ that were enriched relative to the atmosphere. If we employ a theoretical compartmental model to interpret this finding, a possible scenario would involve one pool of centennial to millennially cycling soil C whose signal dominates the $\Delta^{14}C_{bulk}$ signal, and second pool of soil C enriched with C fixed from the atmosphere in the years immediately following the bomb-C spike, e.g. 1964 to 1990, whose signal dominates the $\Delta^{14}C_{respired}$ signal. More complex model structures could potentially be fit to these data, but the data provide clear evidence for the presence of at least two distinct pools with strongly depleted C largely inaccessible to the microbial community, and another pool enriched with decadally cycling C dominating the respiration flux. This stands in contrast to the soils with $\Delta^{14}C_{respired}$ values close to that of the atmosphere, in which the respired signal is likely dominated by sub-decadally cycling C.

Laboratory studies on soil organic matter associations with poorly crystalline metal oxides such as goethite show that only a portion of the organic matter is so tightly bound as to resist desorption (Kaiser and Guggenberger, 2003). Further studies have demonstrated

537  that a portion of the organic matter can be mobilized by exchange with DOC (Leinemann et

538  al., 2018). In this scenario the highly depleted $\Delta^{14}C_{bulk}$ values observed in the soils with high

539  concentrations of poorly crystalline minerals may derive from organic matter that is strongly

540  sorbed or trapped in micropores, while the bomb-C enriched decadally cycling C observed in

541  the respiration flux could derive from the more microbially accessible and DOC-exchangeable

542  mineral associated soil C pool. However, the rates of change over time that we observed for

543  $\Delta^{14}C_{respired}$ indicate that annually cycling C is also an important component of soil organic

544  matter at all of our sites.

545      Our finding that parent material explains more of the variation in $\Delta^{14}C_{respired}$ at depth

546  than climate suggests the role of soil minerals in regulating annually to decadally cycling soil

547  C is of particular importance in deeper soil layers. DOC has been shown to move downward

548  through the soil profile via preferential sorption of new soil C inputs and corresponding

549  desorption of older DOC, which is then available to the microbial community (Kaiser and

550  Kalbitz, 2012). This process is mineral controlled, and while we did not test it directly, such

551  a process could explain why we see an increased importance of parent material, and the

552  interaction between climate and parent material, for explaining $\Delta^{14}C_{respired}$ trends with

553  depth.

554      In contrast to what we observed for the poorly crystalline metal oxides, the lack of

555  correlation we observed between crystalline Fe oxides and soil radiocarbon suggests that

556  these minerals do not play an important role in explaining soil C persistence, at least in

557  these soils. Other studies have shown that crystalline Fe oxides do protect soil C from

558  microbial decomposition, but that the overall sorption capacity of these mineral species is

559  low [Kahle et al., 2003]. We observed a large increase in the amount of iron dissolved from

560  crystalline minerals at the warm sites relative to the cool or cold sites, along with a

561  corresponding decrease in soil C concentration and relative enrichment in both $\Delta^{14}C_{bulk}$ and

562  $\Delta^{14}C_{respired}$. This increase in crystalline iron was also associated with a corresponding

563 decrease in the amount of poorly crystalline minerals. Together these trends suggest that

564 these soils have lost poorly crystalline minerals through leaching and transformation into

565 crystalline species. The patterns of C concentrations and associated SOC stocks, $\Delta^{14}C_{bulk}$,

566 and $\Delta^{14}C_{respired}$ observed across the climate/weathering gradient suggest that weathering of

567 poorly crystalline metal oxides leads to a reduction in soil carbon stocks, which is caused by

568 losses of old $\Delta^{14}C$ depleted carbon associated with these minerals, and that this process is

569 relevant across a range of igneous parent materials.

570      The sensitivity of decomposition to temperature is of particular interest for

571 understanding how soil C dynamics may change under a warming climate. Comparing the

572 change in $\Delta^{14}C_{respired}$ over time for the different climate zones across the different lithologies

573 provides insight into this question. Focusing on the near surface soils (0-0.1 m), where

574 climate effects are strongest, we observed that the rate of change in $\Delta^{14}C_{respired}$ over time

575 was correlated with poorly crystalline metal oxide content. We observed a linear relationship

576 between MAT and the rate of change in $\Delta^{14}C_{respired}$ over time for the granitic soils, which

577 had low concentrations of poorly crystalline metal oxides in all three climate zones. In

578 contrast, $\Delta^{14}C_{respired}$ changed more over time in the coldest climate zone for the basaltic and

579 andesitic soils than in the cool climate zone with higher concentrations of poorly crystalline

580 metal oxides. Furthermore, the change in $\Delta^{14}C_{respired}$ over time was similar for all three

581 parent materials at the warm climate zone with minimal poorly crystalline metal oxide

582 content. These findings provide evidence that the temperature sensitivity of soil organic

583 matter decomposition may be attenuated in the presence of poorly crystalline minerals. If

584 this is true, we would expect that potential increases in decomposition rates, and

585 accompanying carbon losses due to climate warming, would be greater in soils lacking

586 substantial concentrations of poorly crystalline metal oxides than in soils enriched in these

587 minerals.

## Conclusion

589     Our study shows clearly that parent material and climate interact to control soil C

590 dynamics. This interaction was the key to explain trends in $\Delta^{14}C_{bulk}$, which is a proxy for

591 the mean age of soil C, and additionally in $\Delta^{14}C_{respired}$, which reveals the relative

592 contributions of faster or more slowly cycling soil C to respiration. We observed that the

593 trends in both $\Delta^{14}C_{bulk}$ and $\Delta^{14}C_{respired}$ were best explained by climate at the soil surface,

594 but best explained by parent material in deeper soil layers. The overall importance of

595 climate was reflected in the changes in $\Delta^{14}C$ we observed over time, both for bulk C and

596 respired $CO_2$. We saw greater changes at the soil surface than in the deeper layers, and in

597 the highly weathered soils of the warm climate sites than in the poorly developed soils of the

598 cold sites. Yet contrary to the expected temperature-decomposition relationship, we saw the

599 most depleted $\Delta^{14}C_{bulk}$ in the cool climate zone with intermediate MAT, which is also where

600 we saw the least amount of change in $\Delta^{14}C$ over time at all depths.

601     The effect of the interaction between parent material and climate on soil C dynamics is

602 best explained by the development of distinct mineral assemblages via weathering, in

603 particular the formation and subsequent loss of poorly crystalline metal oxides. We confirm

604 the findings of other studies showing that poorly crystalline minerals are highly correlated

605 with the age of soil C, as measured by proxy with $\Delta^{14}C_{bulk}$. We extend this finding to show

606 that it is specifically the poorly crystalline metal oxide content that is correlated with

607 $\Delta^{14}C_{bulk}$, and that the correlation with crystalline Fe content is not significant. Furthermore,

608 we provide mechanistic evidence for the protective effect of mineral-association on

609 decomposition of soil organic matter by demonstrating that the difference between $\Delta^{14}C_{bulk}$

610 and $\Delta^{14}C_{respired}$ is highly correlated with poorly crystalline mineral content. Finally, the

611 time series data of $\Delta^{14}C_{respired}$ provides preliminary evidence that the association of soil

612 organic matter with poorly crystalline metal oxides may attenuate the temperature

613 sensitivity of decomposition.

614    In future work we intend to quantify the timescales of soil carbon cycling in mineral

615 and non-mineral associated pools with a compartmental modeling approach, using the

616 radiocarbon time series presented here in addition to radiocarbon measurements of soil

617 density and thermal fractions as constraints. With this modeling framework we also hope to

618 test additional hypotheses regarding mineral association and temperature sensitivity of soil

619 organic matter.